

Searching for broad-line emitting galaxies with JWST FRESCO data

Songnan QI

Supervisor: : Alba Covelo Paz

Co-supervisor: Pascal Oesch

July 3, 2025



**UNIVERSITÉ
DE GENÈVE**

FACULTY OF SCIENCE

Department of Astronomy

Contents

1	Introduction	1
1.1	Broad-line emitters as Type 1 AGNs	1
1.2	JWST slitless grism spectroscopy	2
1.3	Main motivations of the project	3
2	Selecting broad-line emitting galaxies	5
2.1	Systematic fitting of Paschen-alpha lines	5
2.2	Visual inspections	6
2.3	Matching with HST observations	7
2.4	Selected BL emitters	7
3	BH-to-stellar mass relations	10
3.1	Deriving the BH masses	10
3.2	CIGALE SED fitting	11
3.3	BH-to-stellar mass ratios	15
4	Summary and conclusion	18
5	Acknowledgments	19
	References	19

1 Introduction

1.1 Broad-line emitters as Type 1 AGNs

Active Galactic Nuclei (AGNs) are extremely luminous and compact regions at the center of certain galaxies, powered by the accretion of matter onto supermassive black holes (SMBHs). They emit radiation across the entire electromagnetic spectrum, from radio waves to gamma rays, making them some of the most powerful sources of energy in the universe. The AGN structure typically includes an accretion disk close to the SMBHs, surrounding regions of ionized gas and dust and possible relativistic jets. Investigating AGNs provides invaluable insights into the extreme physics near black holes, the mechanisms behind high-energy photon generation, and their profound impact on the evolutionary pathways of their host galaxies.

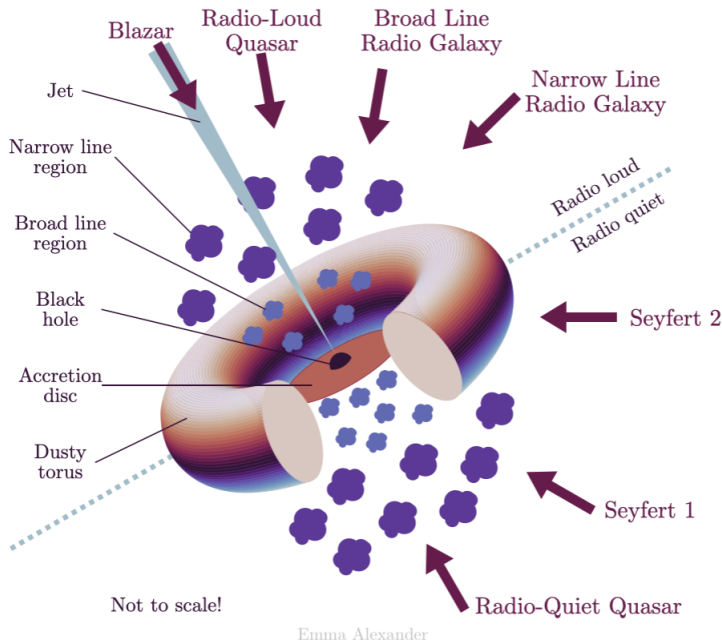


Figure 1: Unified model of AGN adapted from Urry & Padovani (1995), made by Emma Alexander

The unified model of AGNs as illustrated in Figure 1, is a theoretical framework developed by Urry & Padovani (1995)[1] that explains the diverse observational characteristics of AGNs as arising primarily from differences in viewing angle rather than intrinsic physical differences. According to this model, all AGNs share a common central engine (SMBH) surrounded by an accretion disk emitting intense radiation, whose observability is not always ensured. Key components of this model also include a region of fast-moving, high-density ionized gas, the Broad-Line Region (BLR), and a more extended, slower-moving region of lower-density gas, the Narrow-Line Region (NLR). Additionally, a dusty torus-shaped structure obscures the central regions when viewed edge-on, leading to classi-



fication differences: Type 1 AGNs, where the BLR is visible, and Type 2 AGNs, where the torus blocks the emission from BLR, leaving only the NLR observable. The half-opening angle of this torus, defined as the angle between the AGN's central rotational axis and the edge of the torus opening, further modulates observability: a flatter torus with a wider opening is less effective at blocking BLR emission, potentially leading to a higher fraction of Type 2 AGNs (Lawrence 1991[2]). Further variations arise from the presence of a relativistic jet: when it's aligned with our line of sight, it produces a blazar with extreme variability and polarization due to the relativistic beaming effect. The Unified Model successfully reconciles many AGN classifications under a single physical scheme, though additional factors like black hole (BH) mass, accretion rate, and host galaxy environment also contribute to the observed diversity.

Broad-line emitting galaxies (BL emitters) serve as crucial laboratories for studying the interplay between AGNs and their host galaxies. These systems are typically identified by the presence of Type 1 AGNs, characterized by their broad emission lines. As detailed in Table 1, these AGNs can be further categorized based on their radio emission properties, luminosities, and radio continuum shapes. Despite these sub-classifications, all BL emitters share a fundamental spectral characteristic: in addition to narrow emission lines indicative of ongoing star formation within the host galaxy, the hydrogen emission lines from the AGN are substantially broadened. This broadening is a direct consequence of the rapid, Doppler-shifted motion of gas within the BLR, a dense turbulent environment surrounding the central SMBH, where photons are emitted through recombination and de-excitation processes.

	Radio-loud	Radio-quiet
Low luminosity	Broad-Line Radio Galaxies (BLRG)	Seyfert 1
High luminosity	Radio-loud quasars, including Steep Spectrum Radio Quasars (SSRQ) and Flat Spectrum Radio Quasars (FSRQ)	Quasar-stellar Objects (QSO)

Table 1: Classification of type 1 AGNs[1]

1.2 JWST slitless grism spectroscopy

The emergence of advanced telescopes with higher resolution is revolutionizing our vision and understanding of the universe, especially at higher redshifts. At the forefront of this revolution stands the James Webb Space Telescope (JWST), an ambitious international collaboration involving NASA, ESA, and CSA. Representing the zenith of space observatory engineering, JWST features a massive 6.5-meter primary mirror, making it the most powerful and largest telescope ever deployed in space. Its core design philosophy centers on exploring the universe across infrared (IR) wavelengths, achieving unparalleled sensitivity and angular resolution. Launched in December 2021, JWST's suite of advanced instruments including NIRCam, NIRSpec, MIRI, and NIRISS enables detailed spectroscopic and imaging studies of distant galaxies, exoplanets, and stellar systems.



Unlike its predecessor, the Hubble Space Telescope (HST), JWST operates primarily in the near-to-mid-infrared (0.6–28 μm), allowing it to peer through cosmic dust and observe high-redshift objects, including some of the earliest galaxies and AGNs.

JWST's NIRISS & NIRCam instruments employ grisms, an optical component combining a diffraction grating and a prism that is used in spectroscopy to disperse light into its constituent wavelengths while maintaining imaging capabilities. Unlike traditional slit-based spectrographs that demand precise target alignment, grisms facilitate slitless spectroscopy, allowing for the simultaneous acquisition of spectra from every object across a wide field of view without the need for narrow apertures. This innovative design means a single astronomical camera can function interchangeably as both a high-resolution imager (when the grism is bypassed) and an efficient spectrograph (when the grism is inserted), eliminating the need for complex mechanical reconfigurations.

Grisms onboard JWST are exquisitely well-suited for searching for broad-line emitting galaxies for two critical reasons:

1. Simultaneous multi-object spectroscopy: Through the implementation of slitless spectroscopy, JWST's grism instruments provide an unparalleled capability: the simultaneous acquisition of a spectrum for every celestial object within the wide field of view. This inherent parallel data collection profoundly boosts observational efficiency, allowing for the discovery and characterization of a large number of faint distant sources including rare or transient BL emitters, without the need for time-consuming pre-selection.
2. High IR sensitivity: A key advantage for studying distant broad-line emitting galaxies lies in JWST's profound sensitivity in the IR. As light from these galaxies travels across the expanding universe, their characteristic emission lines are stretched into the portion of the spectrum at longer (NIR-MIR) wavelengths. JWST's instruments, particularly NIRCam with its integrated grism mode, are meticulously designed for high sensitivity in these IR wavelengths, enabling the robust detection of one or more of these diagnostic lines whenever they fall within the instrument's spectral range.

1.3 Main motivations of the project

According to the unified model of AGNs, BL emitters are generally observed to be relatively rare. This rarity stems from two observational challenges: the distinct signature of the BLR can be substantially diluted by the light of the host galaxy, or it can be completely obscured by an optically thick dusty torus. The detectability of BL emitters is thus linked to its orientation relative to our line of sight, as well as the structure of the obscuring torus itself. Given these challenges, the discovery and detailed study of BL emitters is of immense scientific interest, offering the potential for breakthrough understanding of their intrinsic physics and their role in cosmic evolution.

During this project, I focused on the data of the JWST FRESCO (First Reionization



Epoch Spectroscopically Complete Observations) survey, which combines direct imaging with slitless grism spectroscopy with the F444W filter, as shown in Figure 2. The NIRCam camera is equipped with two grisms at long wavelengths: GrismR and GrismC, with a difference in dispersion direction of 90 degrees. FRESCO uses GrismR to disperse all light in the field without specific targeting and create 2D spectra for each object, and the 1D spectra are obtained by collapsing the 2D spectra along the spatial axis. Using this technique, the FRESCO survey provides us with high resolution ($R \sim 1600$) spectra at $3.8\text{-}5.0\mu\text{m}$ covering the majority of GOODS-N and GOODS-S fields.

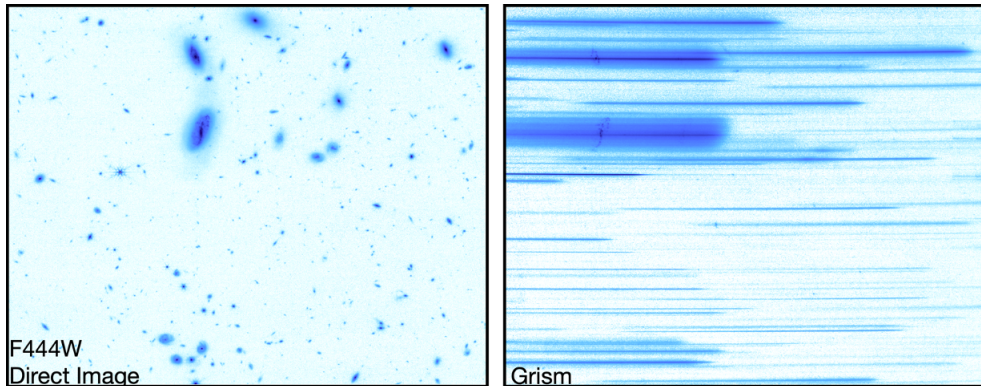


Figure 2: Example of FRESCO’s spectroscopic strategy[3]. Left: a part of the F444W direct image in the FRESCO-S field. Right: the spectra of each galaxy on the same image as the left panel, obtained with light dispersed by the GrismR

This project aimed to find BL emitters within the redshift range $z \sim 1\text{-}1.7$, close to the peak of the cosmic star formation history, among the galaxies detected by JWST FRESCO survey. The Paschen-alpha ($\text{Pa}\alpha$) lines of these galaxies at rest-frame wavelength $\lambda_0 = 1875.2\text{nm}$ would be observed at $3.8\text{--}5.0\mu\text{m}$, which is beyond the detectability of Hubble Space Telescope (HST), yet can be observed by JWST with better resolution. By analyzing the emission line profiles, BH masses of galaxies were constrained. I also applied the SED fitting code CIGALE to estimate the total stellar masses of the identified BL emitters, which enabled a comparison between the resulting BH-to-stellar mass ($M_{\text{BH}} - M_{\star}$) relations and those from previous researches, contributing to the study of the coevolution of the SMBH with its host galaxy.

2 Selecting broad-line emitting galaxies

2.1 Systematic fitting of Paschen-alpha lines

The galaxy sample comprises 897 sources (405 from GOODS-N and 492 from GOODS-S) at redshifts $z \sim 1$ –1.7 with signal-to-noise ratios (S/N) > 10 in the FRESCO data. The 1D spectra were extracted from the 2D slitless spectra using **GRIZLI** (Grism Redshift and Line Analysis), a specialized pipeline designed to process slitless spectroscopic data from space telescopes. It accounts for contamination from overlapping spectra, fits the 1D spectra, and robustly estimates associated errors.

Once 1D spectra were recovered, the $\text{Pa}\alpha$ lines of all sources were identified at $\lambda_{\text{obs}} = \lambda_0 \cdot (1 + z)$, and the wavelengths on the x-axis of the spectra were converted to Doppler velocities centered on the $\text{Pa}\alpha$ line by the following relation.

$$v = c \left[\frac{\lambda_{\text{obs}}}{(1 + z)\lambda_0} - 1 \right] \quad (1)$$

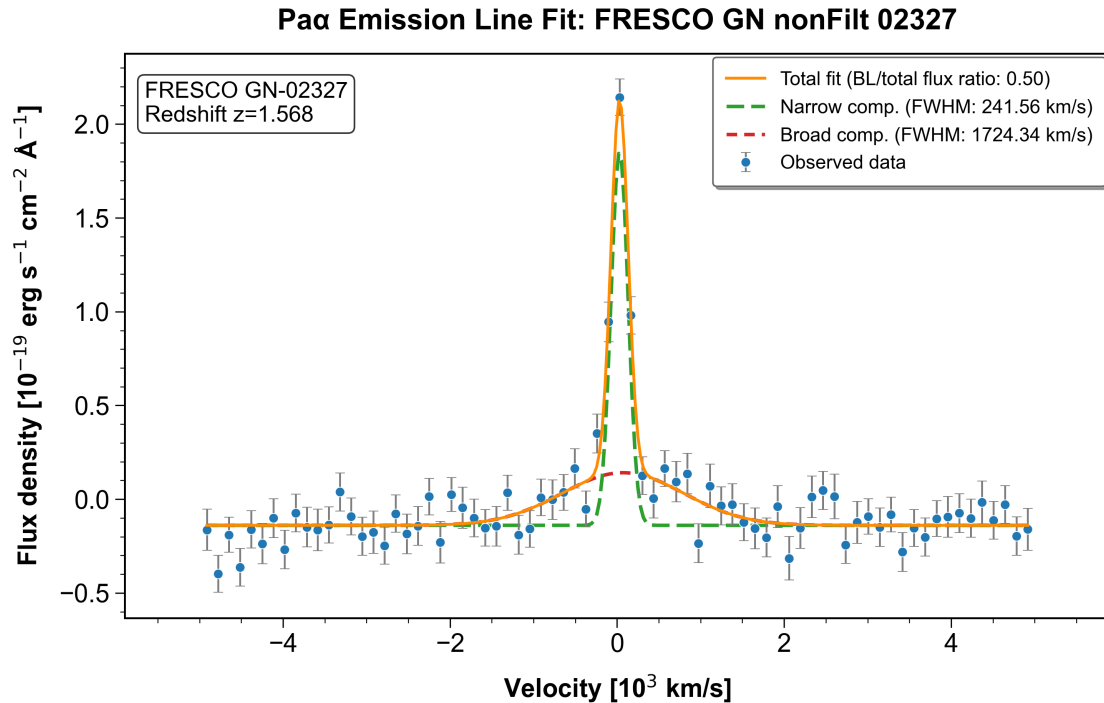


Figure 3: Paschen-alpha emission line fitting of GN-02327

I then used the Python package `lmfit` to perform multi-component Gaussian fittings systematically for each source, by considering the combination of a narrow Gaussian component, a broad Gaussian component and a constant continuum. Galaxies with $\text{Pa}\alpha$ emission lines fitted with a broad-line component $\text{FWHM}_{\text{BL}} > 1000$ km/s and a broad-line

(BL) flux contribution $> 50\%$ were classified as candidates for BL emitters and advanced to the next selection stage. An example is shown in figure 3, which displays one of the confirmed BL emitters identified in this study. Its narrow-line (NL) component exhibits a FWHM < 500 km/s, consistent with gas kinematics driven by star formation in galaxies.

2.2 Visual inspections

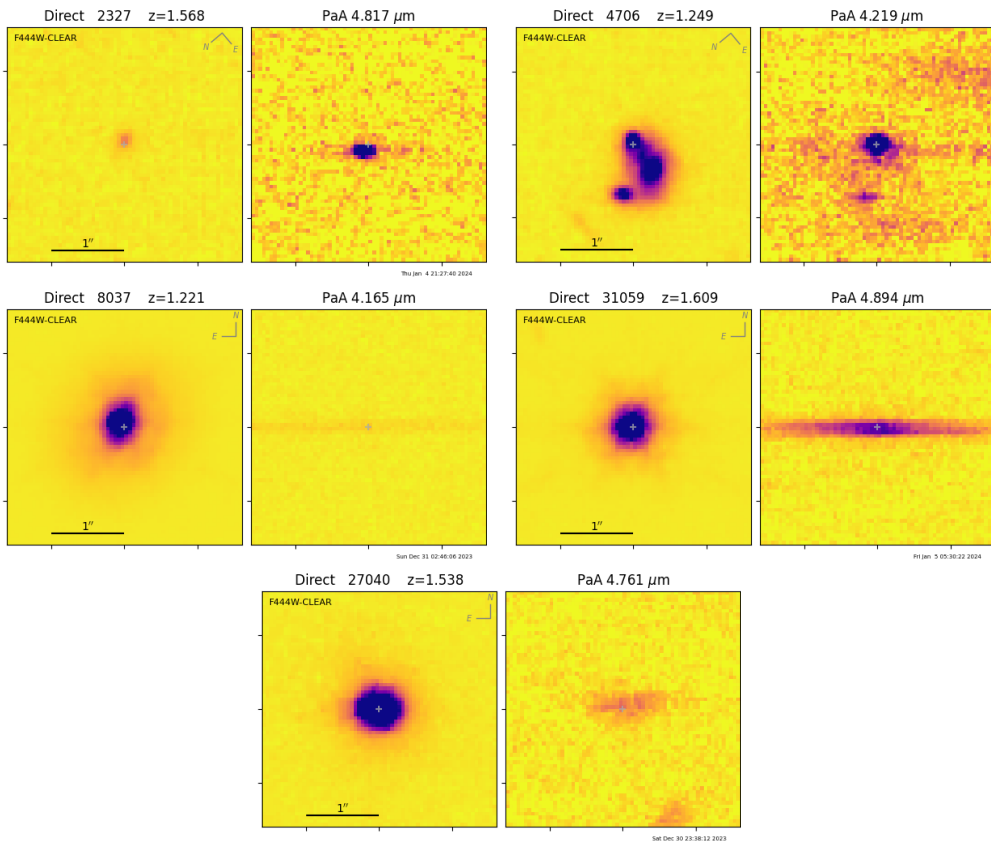


Figure 4: Direct images and 2D spectra of the selected BL emitters: GN-02327, GN-04706, GS-08037, GS-31059, GS-27040

The previous step reduced the number of candidates to approximately 260, which was further reduced by visual inspection. I inspected the direct images and 2D slitless spectra one by one to check if they meet the conditions for BL emitters:

- In direct images, they should look like round compact sources since the BLR dominates the emission.
- In 2D spectra, they should exhibit a significant broad component, i.e. a thin line centered at the point source and elongated along the direction of dispersion.

Many candidates were rejected during this stage because of contamination or the absence of a clear BL component in their spectra, leaving a final sample of 10 candidates of

high-confidence.

2.3 Matching with HST observations

The last step before confirming BL emitters was to search for HST observations of the same sources. Up to this stage, there was only one source that has met all features expected for a BL emitter, and thus confirmed even without precedent HST spectral data. For the other nine candidates, their coordinates on the sky (RA and Dec) were used to query the Mikulski Archive for Space Telescopes (MAST) and to identify their precise target fields. From the archival catalog of each field, objects with consistent redshifts and positional offsets < 0.4 arcsec relative to the JWST coordinates were selected. Then I examined HST spectroscopic data (Momcheva et al. 2015[4], Brammer et al. 2012[5]) to verify the presence of broadened emission lines, especially broadened H α line in these matched spectra.

2.4 Selected BL emitters

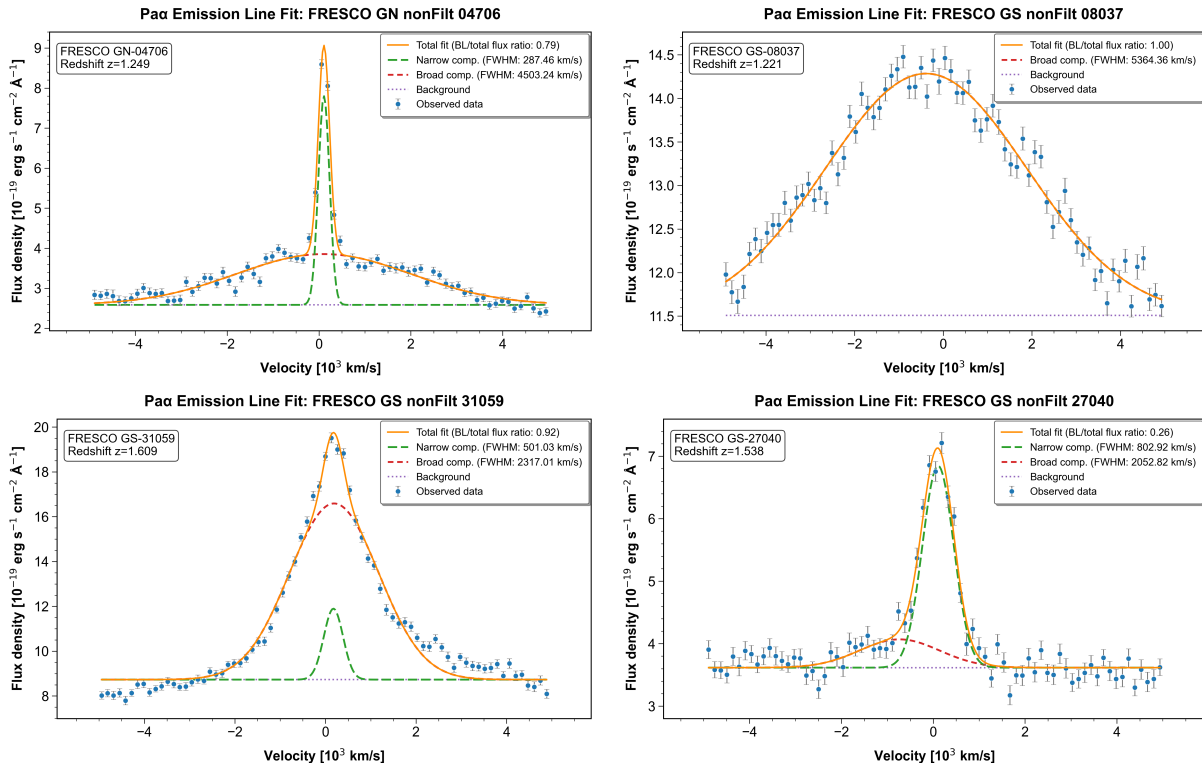


Figure 5: FRESCO data with multi-component Gaussian fits of GN-04706, GS-08037, GS-31059, GS-27040

The five BL emitters confirmed by this study are presented with their direct images and 2D spectra in Figure 4, FRESCO data with multi-component Gaussian fits in Figure

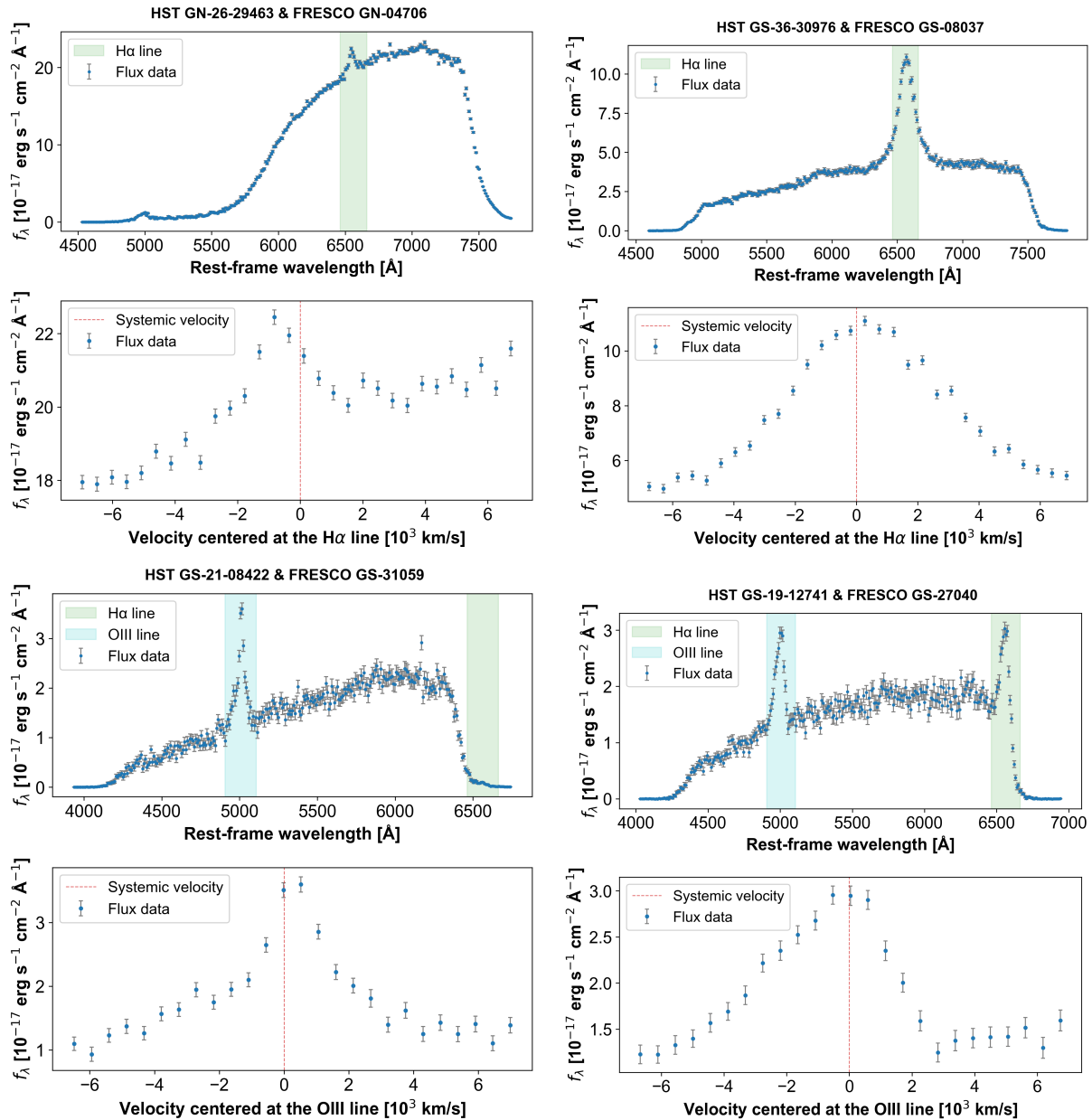


Figure 6: HST spectral data of GN-04706, GS-08037, GS-31059, GS-27040



3.5 and matched HST spectra in Figure 6.

1. **GN-02327:** Among the five identified BL emitters, this source displays the most canonical properties: a BL component with $\text{FWHM}_{\text{BL}} = 1724 \text{ km/s}$ contributing 50% of the total flux, both NL and BL components symmetrically centered on Paschen-alpha, and a broadened $\text{H}\alpha$ line in HST spectrum confirming its BL nature.
2. **GN-04706:** This source exhibits a typical NL component accompanied by an exceptionally broad emission line with $\text{FWHM}_{\text{BL}} = 4503 \text{ km/s}$, indicative of a fast rotating BLR around the SMBH. The direct image reveals three spatially proximate sources, one of which is absent in the 2D slitless spectrum, suggesting a distinct redshift for this object. The presence of a clearly broadened $\text{H}\alpha$ emission line in its HST 1D spectrum confirms this source as a BL emitter.
3. **GS-08037:** Given the spectrum's complete dominance by emission from the BLR, I performed a two-component Gaussian fit (BL + continuum), yielding an exceptionally high $\text{FWHM}_{\text{BL}} = 5364 \text{ km/s}$ which is the largest among the five BL emitters. The source's quasar nature is further evidenced by the distinctive hexagonal point-spread function (PSF) in direct imaging, characteristic of JWST's 18-segment hexagonal primary mirror which creates 6 diffraction spikes for bright point sources.
4. **GS-31059:** The source displays a conventional BL component ($\text{FWHM}_{\text{BL}} = 2317 \text{ km/s}$) and an NL component at the upper limit of NL classification ($\text{FWHM}_{\text{NL}} = 500 \text{ km/s}$). Although $\text{H}\alpha$ is undetectable by HST at $z = 1.609$, the observed [OIII] emission shows potential broadening, though this could alternatively represent an unresolved doublet ([OIII] $\lambda 4959$, [OIII] $\lambda 5007$). The JWST direct image reveals the hexagonal PSF characteristic of luminous quasars, confirming its AGN nature.
5. **GS-27040:** This source was excluded from the candidate list based on systematic multi-component Gaussian fitting, as its NL component ($\text{FWHM}_{\text{NL}} = 803 \text{ km/s}$) is significantly broader than the typical values for star-forming regions, and its BL flux ratio of 26% is below the selection threshold. Additionally, its 2D spectrum lacks a clear BL component. However, Sun et al. (2024)[\[6\]](#) classified it as a BL emitter, reporting an intrinsic Pa α $\text{FWHM}_{\text{BL}} = 1821 \pm 259 \text{ km/s}$. I thus retained it in my analysis, as the NL emission may instead originate from the BLR, while the BL component could arise from a high-velocity outflow with $\text{FWHM}_{\text{BL}} = 2053 \text{ km/s}$ driven by AGN feedback. This scenario is further supported by a redshift offset $\Delta z = 7.4 \cdot 10^{-6}$ between the BL component and the Pa α line, likely due to outflow kinematics and minor galaxy asymmetry. Although its $\text{H}\alpha$ line is broadened, its detection at the sensitivity limit of HST reduces its reliability as a diagnostic.

Based on Seymour et al. in prep., both FRESCO GS-08037 and FRESCO GS-31059 have been detected in Chandra X-ray observations, with the latter also exhibiting radio emission. These multi-wavelength detections provide robust evidence for quasar activity, powered by accretion onto a central SMBH.



3 BH-to-stellar mass relations

With the identification of five BL emitters secured, I characterized their fundamental physical properties, particularly their BH masses (M_{BH}) and total stellar masses (M_{\star}). The M_{BH} can be estimated from Pa α emission line properties, combining its luminosity ($L_{\text{Pa}\alpha}$) and velocity width (FWHM $_{\text{Pa}\alpha}$). Meanwhile, M_{\star} can be constrained through spectral energy distribution (SED) fitting using codes like CIGALE, which model the stellar populations by fitting multi-wavelength photometry.

These measurements enable the construction of the $M_{\text{BH}}-M_{\star}$ relation for my BL emitter sample, providing crucial insights into the coevolution of supermassive black holes and their host galaxies at redshifts ranging from 1 to 1.7, bridging the gap between the high redshift and local universe. Such analysis may reveal whether these systems follow local scaling relations or exhibit deviations suggestive of different growth histories.

3.1 Deriving the BH masses

Building upon the foundational work of Greene & Ho (2005)[7], who established BH mass estimators for AGNs using the luminosity ($L_{\text{H}\alpha}$) and velocity width (FWHM $_{\text{H}\alpha}$) of the H α emission line, Kim et al. (2010)[8] developed a novel calibration based on Pa α line properties. Leveraging the well-documented correlations between $L_{\text{H}\alpha}$ and $L_{\text{Pa}\alpha}$ and between FWHM $_{\text{H}\alpha}$ and FWHM $_{\text{Pa}\alpha}$, they derived a relation taking the form of Eq. 2:

$$\log M = a + b \log L_{\text{Pa}\alpha} + c \log \text{FWHM}_{\text{Pa}\alpha} \quad (2)$$

Three sets of parameters (a, b, c) were found by different methods:

1. The luminosity and FWHM of H α line were replaced with their Pa α counterparts using empirical scaling relations.
2. Following the theoretical expectation from the virial theorem ($c = 2$), the coefficients a and b in the relation 2 were solved by performing a linear regression fit.
3. All the three parameters (a, b, c) are treated as free parameters in a multiple variable linear regression fit.

with the values below.:

$$\frac{M}{M_{\odot}} = 10^{7.29 \pm 0.10} \left(\frac{L_{\text{Pa}\alpha}}{10^{42} \text{erg s}^{-1}} \right)^{0.43 \pm 0.03} \left(\frac{\text{FWHM}_{\text{Pa}\alpha}}{10^3 \text{ km s}^{-1}} \right)^{1.92 \pm 0.18} \quad (3)$$

$$\frac{M}{M_{\odot}} = 10^{7.16 \pm 0.04} \left(\frac{L_{\text{Pa}\alpha}}{10^{42} \text{erg s}^{-1}} \right)^{0.49 \pm 0.06} \left(\frac{\text{FWHM}_{\text{Pa}\alpha}}{10^3 \text{ km s}^{-1}} \right)^2 \quad (4)$$

$$\frac{M}{M_{\odot}} = 10^{7.31} \left(\frac{L_{\text{Pa}\alpha}}{10^{42} \text{erg s}^{-1}} \right)^{0.48 \pm 0.03} \left(\frac{\text{FWHM}_{\text{Pa}\alpha}}{10^3 \text{ km s}^{-1}} \right)^{1.68 \pm 0.12} \quad (5)$$



I decided to estimate the BH masses using all three relations and accept the results with the smallest uncertainties. The flux measurements were converted into L_{Pa} by assuming a standard Λ CDM cosmology of $H_0 = 70 \text{ km/s/Mpc}$, $\Omega_m = 0.3$ and $\Omega_\Lambda = 0.7$, and FWHM_{Pa} are given by the Gaussian fits of BL component in the section 2.1.

3.2 CIGALE SED fitting

Code for Investigating GALaxy Emission (CIGALE) is a powerful SED fitting code designed to model the FUV-to-radio emission of galaxies by combining stellar, dust, AGN, and gas components which are modeled in separate modules. Developed by Boquien et al. (2019)[9], CIGALE employs a Bayesian approach to derive physical properties of galaxies, such as stellar masses, star formation rates (SFRs), dust attenuation and AGN contributions based on multi-wavelength photometric data.

The modules that I employed are:

- `sfhdelayedbq` for star formation history (SFH), which allows for a smooth increase of SFR after the onset of star formation and avoids extreme bursts.
- `bpassv2` for stellar populations, which is the version 2.2 of the Binary Population And Spectral Synthesis (BPASS) model[10]. It incorporates binary stellar evolution pathways which have significant effects on the lifetimes, temperatures, gravities, and integrated light properties of stars.
- `nebular` for nebular emission, which adopted metallicity-dependent nebular templates presented by Inoue (2011)[11]. Emissivities of emission lines relative to H β are provided for nebular line emissions, and bound-free, free-free as well as two-photon hydrogen emissions are considered for nebular continuum.
- `dustatt_modified_starburst` for dust attenuation, which modifies the slope of the continuum emission by a power law function.
- `skirtor2016` for AGN, which implements a physically-motivated model for AGN emission, featuring a clumpy two-phase dusty torus structure as developed by Stalevski et al. (2016)[12]. This advanced treatment incorporates wavelength-dependent 3D Monte Carlo radiative transfer calculations using `skirt` and can better reproduce observed AGN spectral features across different inclination angles.

With all modules above parametrized, I performed SED fitting for all the five BL emitters. The filters of photometric data that were fed to CIGALE before fitting were listed in Table 2. HST fluxes were excluded for the fitting of GS-08037 since they exceeded the values of the fluxes obtained from JWST filters, with which a good fit could not be achieved. The reduced χ^2 are < 1 for all of the five BL emitters I've identified, implying a slight over-fitting issue.



HST filters	JWST filters
hst.acs.wfc.F435W	jwst.nircam.F090W
hst.acs.wfc.F606W	jwst.nircam.F115W
hst.acs.wfc.F775W	jwst.nircam.F150W
hst.acs.wfc.F814W	jwst.nircam.F182M
hst.wfc3.ir.F105W	jwst.nircam.F200W
hst.wfc3.ir.F125W	jwst.nircam.F210M
hst.wfc3.ir.F140W	jwst.nircam.F277W
hst.wfc3.ir.F160W	jwst.nircam.F335M
	jwst.nircam.F356W
	jwst.nircam.F410M
	jwst.nircam.F444W

Table 2: Filters of the photometric data

Figure 7, 8 displays the best-fit SEDs obtained for all of the 5 BL emitters. Each model spectrum (black line) comprises three key components: an AGN component (orange), nebular emission (green), and attenuated stellar emission (yellow). The close agreement between the observed photometric fluxes (purple empty circles) and the model-predicted fluxes (red filled circles) indicates good fits. Discrepancies where observed fluxes appear higher than the model spectrum are often attributed to broad filters that encompass strong emission lines.

Taking FRESCO GN-04706’s best-fit SED as a prime illustration, distinct spectral features are noticed. The most luminous line is the unresolved [OIII] $\lambda 4959, \lambda 5007$ doublet, a key diagnostic of gas metallicity and ionization state, often indicative of an AGN or vigorous star formation. Following in intensity is the H α line, a primary tracer of the star formation rate. Furthermore, the Pa α line is clearly present in IR at approximately $4.2\mu\text{m}$, offering crucial information on ionized gas in dust-obscured regions.

Upon inspection, the BL emitters within GOODS-N and GOODS-S reveal contrasting spectral characteristics related to dust content, likely by chance. The two BL emitters in GOODS-N are characterized by a nearly flat continuum, which strongly implies a lack of significant dust attenuation. This suggests that these objects are either intrinsically dust-poor or seen along particularly clear lines of sight. Conversely, the three BL emitters residing in GOODS-S are characterized by continua exhibiting notable positive slopes. This spectral reddening is a direct consequence of significant dust attenuation, which not only decreases the visibility of their intrinsic emission lines but can also lead to the appearance of strong absorption lines as light from SMBH passes through dusty foreground material.

It’s important to acknowledge that SED fitting often faces significant degeneracies. These arise from the substantial number of free parameters involved and the fact that several parameters can produce similar effects on the observed SED. This means that different combinations of physical parameters might yield equally good statistical fits, making it challenging to uniquely constrain individual properties.

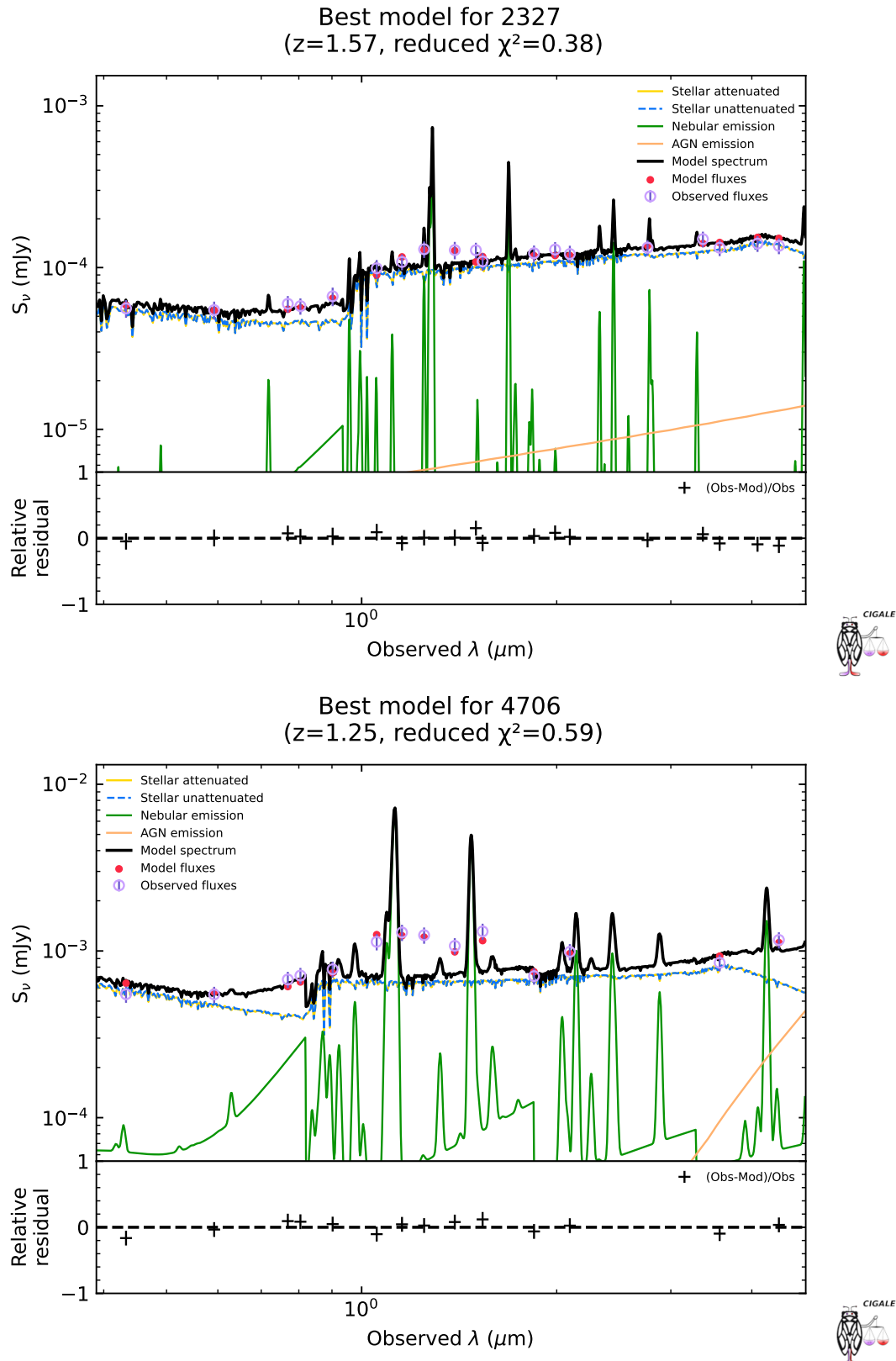


Figure 7: Fit spectra of FRESCO GN-02327, GN-04706 using CIGALE

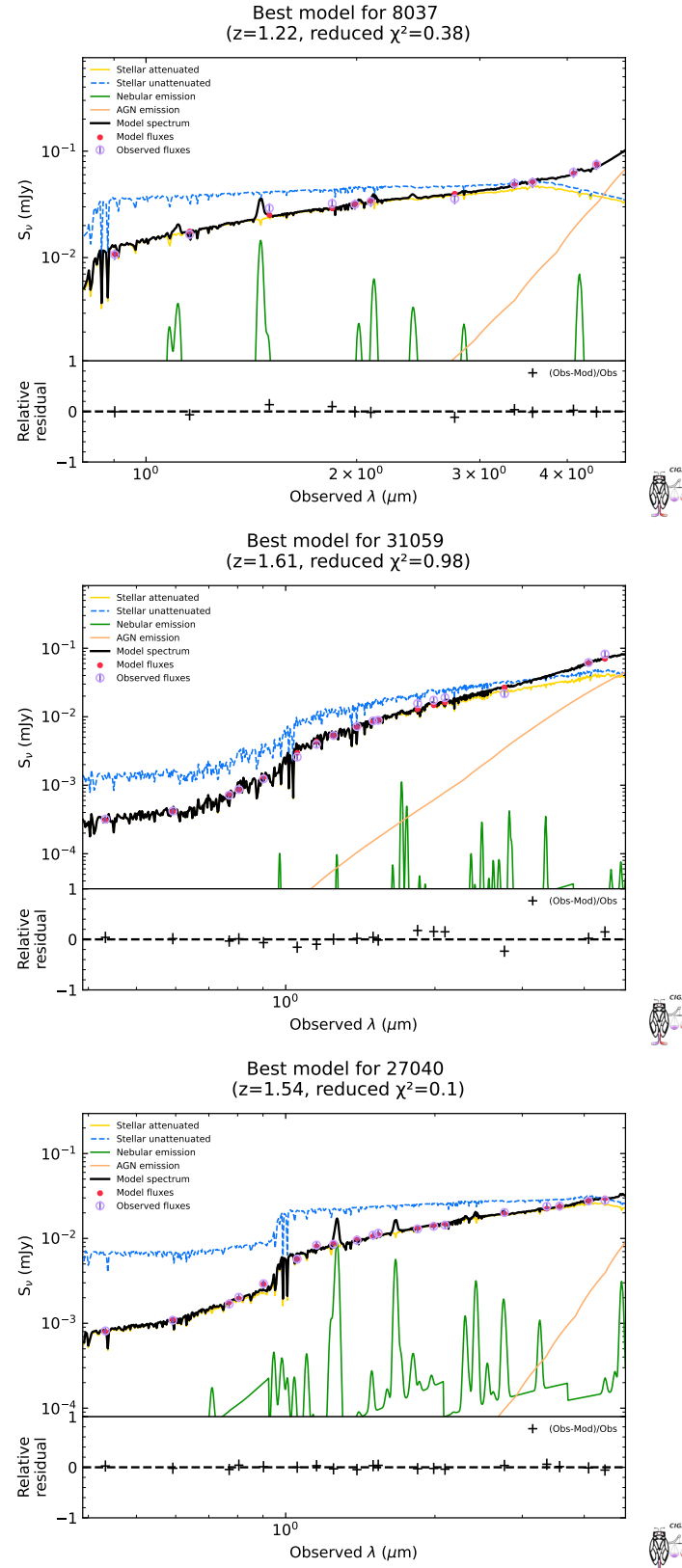


Figure 8: Fit spectra of FRESCO GS-08037, GS-31059, GS-27040 using CIGALE

Fortunately, the only physical quantity required for this study was the total stellar mass, and I found that M_* does not vary much even when the parameter spaces were modified or different degenerate solutions were explored. This robustness in stellar mass determination, despite the inherent degeneracies in other parameters, provides confidence in my results.

3.3 BH-to-stellar mass ratios

With the BH masses obtained from the $\text{Pa}\alpha$ line properties in section 3.1 and the total stellar masses of galaxies estimated from CIGALE SED fitting in section 3.2, the $M_{\text{BH}}-M_*$ relations are established as shown in Figure 9.

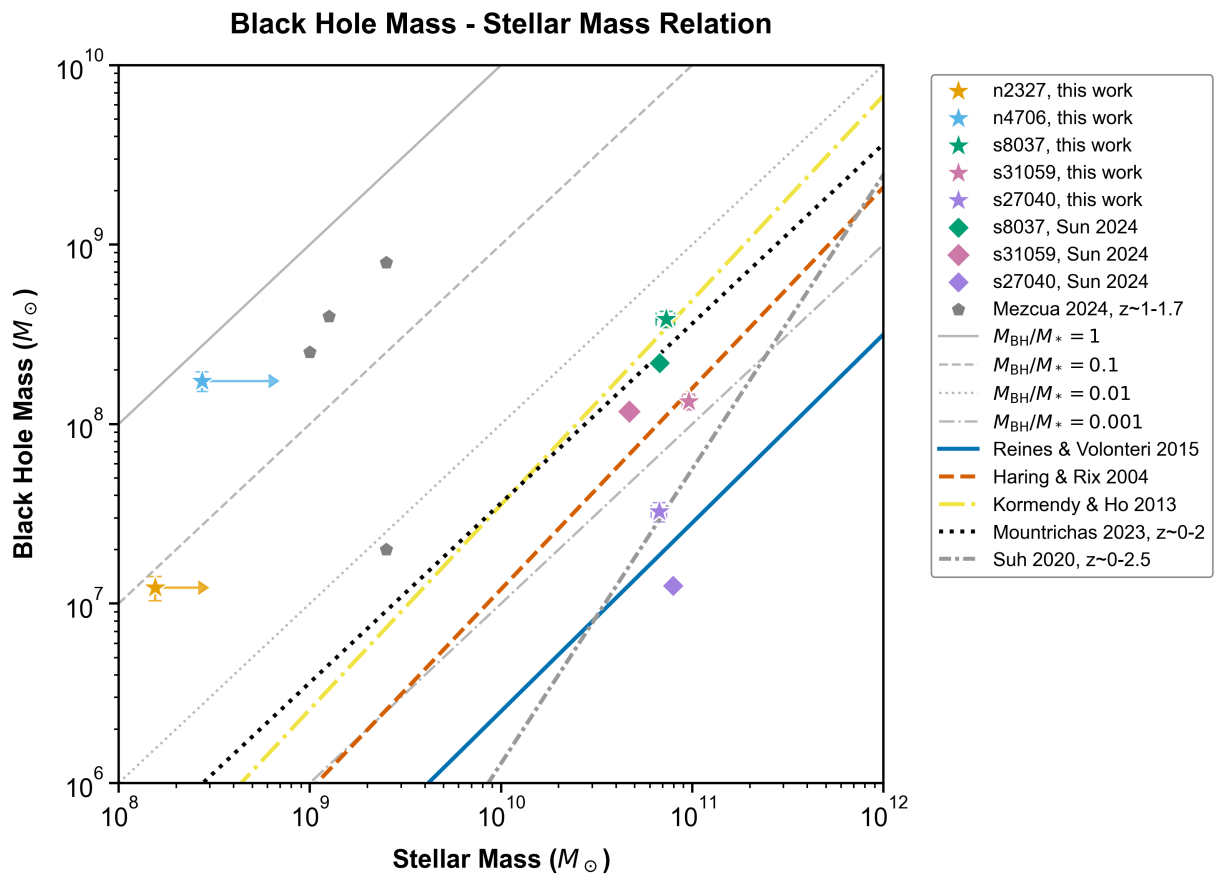


Figure 9: BH-stellar mass relations

Some literature scaling relations are also given on the same plot:

- Häring & Rix (2004)[13] established the relation between M_{BH} and the stellar mass of the bulge M_{bulge} based on a sample of 30 nearby galaxies. The range of M_{bulge}/M_\odot extended from 10^9 to 10^{12} .



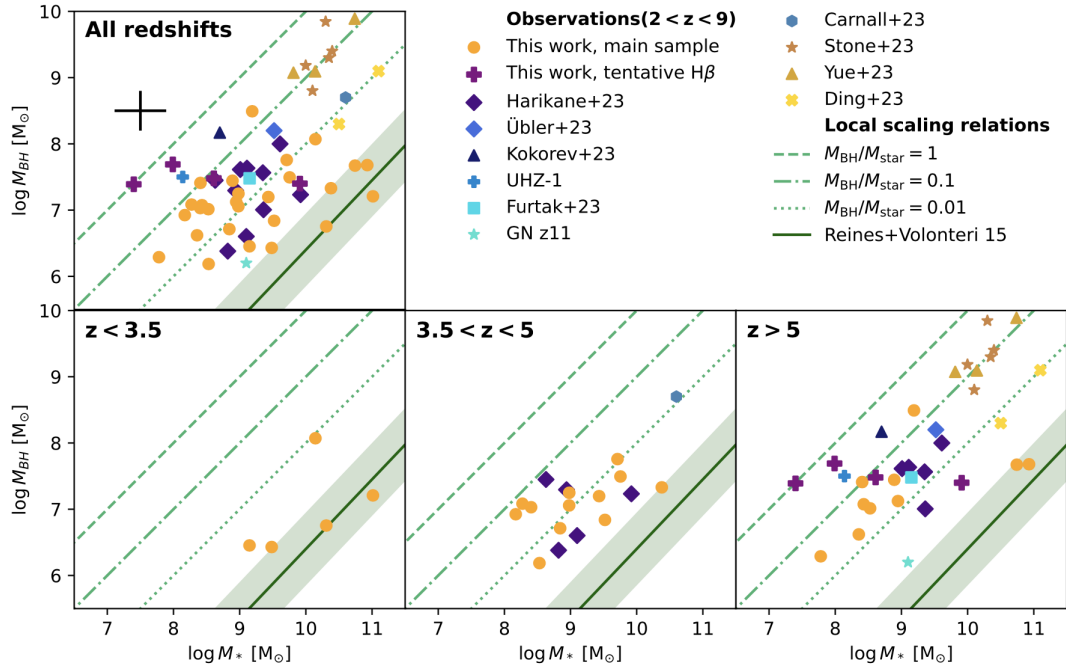
- Kormendy & Ho (2013)[14] found the $M_{\text{BH}}-M_{\text{bulge}}$ relation from 14 S0 galaxies and 12 additional galaxies hosting BHs in the local universe.
- Reines & Volonteri (2015)[15] derived the scaling relation from 262 Type 1 AGNs in the local universe ($z < 0.055$) and 79 galaxies with known dynamical M_{BH} .
- Mountrichas (2023)[16] studied the $M_{\text{BH}}-M_{\star}$ relation based on 687 X-ray luminous Type 1 AGNs at $z \sim 0.2-4.0$, since it's hard to distinguish the bulge from the total stellar mass for high redshift galaxies.
- Suh et al. (2020)[17] suggested a scaling relation by studying 100 X-ray-selected moderate-luminosity Type 1 AGNs at $z < 2.5$.

Other BL emitters from two recent studies are plotted: the sources from Sun et al. (2024) are represented by colored rhombi, while those from Mezcua et al. (2024)[18] are shown as gray pentagons. It's worth noting that the three galaxies from Sun et al. (2024) on the plot are, in fact, the same sources I've independently found in the GOODS-S field. This provides a valuable point of cross-validation for my detections. Furthermore, the four galaxies from Mezcua et al. (2024) that fall within the redshift range of $z \sim 1-1.7$ exhibit approximately the same scaling relation as FRESCO GN-02327 and GN-04706.

Upon examining the five BL emitters, it is immediately noticed that they fall into two distinct M_{BH}/M_{\star} scaling relations. One group aligns well with five established literature relations from the local universe, suggesting these galaxies follow expected co-evolutionary trends between their SMBHs and host stellar bulges.

However, the second group presents a notable departure, showing a significantly higher M_{BH}/M_{\star} ratio, which appears to be unrealistic. This finding contrasts with studies by Mountrichas (2023) and Suh et al. (2020), which generally do not support significant evolution in the M_{BH}/M_{\star} relation out to redshift $z=4$. Juodžbalis et al. (2025)[19] reported a significant evolution in the $M_{\text{BH}}-M_{\star}$ relation, with progressively higher ratios at $z < 3.5$, $3.5 < z < 5$, and $z > 5$. Intriguingly, the second group in my sample exhibits a scaling relation closely resembling their $z > 5$ systems as shown in Figure 10, challenging standard coevolution models and highlights the potential diversity of BH-galaxy growth pathways.

The exact reason for this second outlier group remains an active area of debate. The outshining effect (Giménez-Arteaga et al. 2024[20]) in SED fitting, due to the fact that young stellar populations dominate emitted fluxes and hide the underlying old stars, could bias M_{\star} low by ~ 0.5 dex. While this could partially explain the offset, it cannot fully account for the observed scatter of this second group from the local scaling relations.


 Figure 10: $M_{\text{BH}} - M_*$ relation given in Juodzbalis et al. (2025)[19]

Another compelling possibility, put forth by Ferré-Mateu et al. (2018)[21], posits the existence of low-mass galaxies hosting overmassive black holes. This scenario could arise from tidal or ram-pressure stripping especially close to the cosmic noon, processes that cause galaxies to lose a substantial portion of their stellar mass while their central BHs remain largely unaffected.

Further contributing to this discussion, Mezcua et al. (2023)[22] suggest that these galaxies might be progenitors of today's massive galaxies, originating from early universe direct collapse BH seeds with M_{BH}/M_{\odot} ranging from 10^2 to 10^5 . These early seeds tend to grow faster than host galaxies, leading to overmassive BHs.

Understanding the nature of this second group is crucial for refining the models of galaxy and BH co-evolution, particularly in the context of different SMBH forming mechanisms and environmental effects.



4 Summary and conclusion

In this project, I started by searching for broad-line emitting galaxies at redshifts around $z \sim 1-1.7$ using grism data from the JWST FRESCO survey. My methodology involved a multi-pronged approach: systematic multi-component Gaussian fitting of Paschen-alpha emission lines, careful visual inspection of both direct images and 2D spectra, and crucial cross-matching with archival Hubble Space Telescope (HST) observations for robust confirmation.

My sample of five confirmed BL emitters includes FRESCO GN-02327, GN-04706, GS-08037, GS-31059, and GS-27040. It's important to note that the latter four sources received additional validation through their corresponding HST observations. These galaxies typically exhibit broad emission lines with $\text{FWHM}_{\text{BL}} \sim 1000-5000 \text{ km/s}$, characteristic of Type 1 AGNs.

Following their identification, I proceeded to estimate the SMBH masses of these galaxies, primarily relying on the properties of their $\text{Pa}\alpha$ lines. Concurrently, their total stellar masses were determined through SED fitting using the CIGALE code. With these crucial physical quantities in hand, I established their M_{BH}/M_{\star} scaling relations and compared them with existing studies.

Three of the identified BL emitters align consistently with the M_{BH}/M_{\star} relations empirically derived for AGNs in the local universe, showing evidence for the co-evolution of SMBHs and their host galaxies. However, the remaining two galaxies present a fascinating offset, suggesting the existence of low-mass galaxies hosting overmassive black holes. This anomaly could potentially be explained by external interactions (e.g., tidal stripping) or by the unusual growth histories of BH seeds in the early universe.

It's important to acknowledge the inherent limitations of this study. My current sample size of only five galaxies is too small to draw definitive conclusions about the physical processes governing AGN and galaxy evolution. Furthermore, our understanding is always susceptible to observational biases. The instruments' magnitude thresholds inherently limit detection capabilities to only the brightest sources. This means that we might be missing a significant population of fainter, yet potentially crucial BL emitting galaxies.

In addition, the selection criterion applied at the beginning could present another source of bias. By imposing a FWHM_{BL} threshold of $>1000 \text{ km/s}$ to ensure that the sources are indeed AGNs and not merely dominated by SF-driven emission, we might inadvertently be biased towards detecting the most massive BHs. This criterion might mean that we are missing a population of BL emitters with smaller BHs.

These selection effects could strongly influence our perception of the true statistical distributions and evolutionary pathways of these objects. To truly unlock the full picture and reveal more exciting statistics of BL emitters, it's imperative that the boundaries of detectability are continuously pushed with future observational campaigns.



5 Acknowledgments

This work is based on observations taken by the 3D-HST Treasury Program (GO 12177 and 12328) with the NASA/ESA HST, which is operated by the Association of Universities for Research in Astronomy, Inc., under NASA contract NAS5-26555.

References

- [1] C. Megan Urry and Paolo Padovani. “Unified Schemes for Radio-Loud Active Galactic Nuclei”. In: *Publications of the Astronomical Society of the Pacific* 107 (Sept. 1995), p. 803. ISSN: 0004-6280, 1538-3873. DOI: [10.1086/133630](https://doi.org/10.1086/133630). URL: <http://iopscience.iop.org/article/10.1086/133630> (visited on 06/30/2025).
- [2] A. Lawrence. “The relative frequency of broad-lined and narrow-lined active galactic nuclei: implications for unified schemes”. In: *Monthly Notices of the Royal Astronomical Society* 252.4 (Oct. 15, 1991), pp. 586–592. ISSN: 0035-8711, 1365-2966. DOI: [10.1093/mnras/252.4.586](https://doi.org/10.1093/mnras/252.4.586). URL: <https://academic.oup.com/mnras/article-lookup/doi/10.1093/mnras/252.4.586> (visited on 07/03/2025).
- [3] P. A. Oesch et al. “The JWST FRESCO survey: legacy NIRCam/grism spectroscopy and imaging in the two GOODS fields”. In: 525.2 (Oct. 2023), pp. 2864–2874. DOI: [10.1093/mnras/stad2411](https://doi.org/10.1093/mnras/stad2411). arXiv: [2304.02026 \[astro-ph.GA\]](https://arxiv.org/abs/2304.02026).
- [4] Ivelina G. Momcheva et al. “A SPECTROSCOPIC SURVEY OF THE FIELDS OF 28 STRONG GRAVITATIONAL LENSES*”. In: *The Astrophysical Journal Supplement Series* 219.2 (Aug. 2015). Publisher: The American Astronomical Society, p. 29. ISSN: 0067-0049. DOI: [10.1088/0067-0049/219/2/29](https://doi.org/10.1088/0067-0049/219/2/29). URL: <https://dx.doi.org/10.1088/0067-0049/219/2/29> (visited on 06/30/2025).
- [5] Gabriel B. Brammer et al. “3D-HST: A Wide-field Grism Spectroscopic Survey with the Hubble Space Telescope”. In: *The Astrophysical Journal Supplement Series* 200 (June 1, 2012). Publisher: IOP ADS Bibcode: 2012ApJS..200...13B, p. 13. ISSN: 0067-0049. DOI: [10.1088/0067-0049/200/2/13](https://doi.org/10.1088/0067-0049/200/2/13). URL: <https://ui.adsabs.harvard.edu/abs/2012ApJS..200...13B> (visited on 06/30/2025).
- [6] Yang Sun et al. “No Evidence for a Significant Evolution of M_{\bullet} – M . Relation in Massive Galaxies up to $z = 4$ ”. In: *The Astrophysical Journal* 978.1 (Jan. 1, 2025), p. 98. ISSN: 0004-637X, 1538-4357. DOI: [10.3847/1538-4357/ad973b](https://doi.org/10.3847/1538-4357/ad973b). URL: <https://iopscience.iop.org/article/10.3847/1538-4357/ad973b> (visited on 07/01/2025).
- [7] Jenny E. Greene and Luis C. Ho. “Estimating Black Hole Masses in Active Galaxies Using the H Emission Line”. In: *The Astrophysical Journal* 630.1 (Sept. 1, 2005). Publisher: IOP Publishing, p. 122. ISSN: 0004-637X. DOI: [10.1086/431897](https://doi.org/10.1086/431897). URL: <https://iopscience.iop.org/article/10.1086/431897/meta> (visited on 07/01/2025).



-
- [8] Dohyeong Kim, Myungshin Im, and Minjin Kim. “NEW ESTIMATORS OF BLACK HOLE MASS IN ACTIVE GALACTIC NUCLEI WITH HYDROGEN PASCHEN LINES”. In: *The Astrophysical Journal* 724.1 (Nov. 20, 2010), pp. 386–399. ISSN: 0004-637X, 1538-4357. DOI: [10.1088/0004-637X/724/1/386](https://doi.org/10.1088/0004-637X/724/1/386). URL: <https://iopscience.iop.org/article/10.1088/0004-637X/724/1/386> (visited on 07/01/2025).
 - [9] M. Boquien et al. “CIGALE: a python Code Investigating GALaxy Emission”. In: *Astronomy & Astrophysics* 622 (Feb. 2019), A103. ISSN: 0004-6361, 1432-0746. DOI: [10.1051/0004-6361/201834156](https://doi.org/10.1051/0004-6361/201834156). URL: <https://www.aanda.org/10.1051/0004-6361/201834156> (visited on 07/01/2025).
 - [10] E R Stanway and J J Eldridge. “Re-evaluating old stellar populations”. In: *Monthly Notices of the Royal Astronomical Society* 479.1 (Sept. 1, 2018), pp. 75–93. ISSN: 0035-8711, 1365-2966. DOI: [10.1093/mnras/sty1353](https://doi.org/10.1093/mnras/sty1353). URL: <https://academic.oup.com/mnras/article/479/1/75/5003394> (visited on 07/01/2025).
 - [11] Akio K. Inoue. “Rest-frame ultraviolet-to-optical spectral characteristics of extremely metal-poor and metal-free galaxies: UV-to-optical spectrum of primordial galaxies”. In: *Monthly Notices of the Royal Astronomical Society* 415.3 (Aug. 11, 2011), pp. 2920–2931. ISSN: 00358711. DOI: [10.1111/j.1365-2966.2011.18906.x](https://doi.org/10.1111/j.1365-2966.2011.18906.x). URL: <https://academic.oup.com/mnras/article-lookup/doi/10.1111/j.1365-2966.2011.18906.x> (visited on 07/01/2025).
 - [12] Marko Stalevski et al. “The dust covering factor in active galactic nuclei”. In: *Monthly Notices of the Royal Astronomical Society* 458.3 (May 21, 2016), pp. 2288–2302. ISSN: 0035-8711, 1365-2966. DOI: [10.1093/mnras/stw444](https://doi.org/10.1093/mnras/stw444). URL: <https://academic.oup.com/mnras/article-lookup/doi/10.1093/mnras/stw444> (visited on 07/01/2025).
 - [13] Nadine Häring and Hans-Walter Rix. “On the Black Hole Mass-Bulge Mass Relation”. In: *The Astrophysical Journal* 604 (Apr. 1, 2004). Publisher: IOP ADS Bibcode: 2004ApJ...604L..89H, pp. L89–L92. ISSN: 0004-637X. DOI: [10.1086/383567](https://doi.org/10.1086/383567). URL: <https://ui.adsabs.harvard.edu/abs/2004ApJ...604L..89H> (visited on 07/01/2025).
 - [14] John Kormendy and Luis C. Ho. “Coevolution (Or Not) of Supermassive Black Holes and Host Galaxies”. In: *Annual Review of Astronomy and Astrophysics* 51 (Volume 51, 2013 Aug. 18, 2013). Publisher: Annual Reviews, pp. 511–653. ISSN: 0066-4146, 1545-4282. DOI: [10.1146/annurev-astro-082708-101811](https://doi.org/10.1146/annurev-astro-082708-101811). URL: <https://www.annualreviews.org/content/journals/10.1146/annurev-astro-082708-101811> (visited on 05/19/2025).
 - [15] Amy E. Reines and Marta Volonteri. “RELATIONS BETWEEN CENTRAL BLACK HOLE MASS AND TOTAL GALAXY STELLAR MASS IN THE LOCAL UNIVERSE”. In: *The Astrophysical Journal* 813.2 (Oct. 29, 2015), p. 82. ISSN: 1538-4357. DOI: [10.1088/0004-637X/813/2/82](https://doi.org/10.1088/0004-637X/813/2/82). URL: <https://iopscience.iop.org/article/10.1088/0004-637X/813/2/82> (visited on 07/01/2025).



- [16] George Mountrichas. “The co-evolution of supermassive black holes and galaxies in luminous AGN over a wide range of redshift”. In: *Astronomy & Astrophysics* 672 (Apr. 1, 2023). Publisher: EDP Sciences, A98. ISSN: 0004-6361, 1432-0746. DOI: [10.1051/0004-6361/202345924](https://doi.org/10.1051/0004-6361/202345924). URL: <https://www.aanda.org/articles/aa/abs/2023/04/aa45924-23/aa45924-23.html> (visited on 05/19/2025).
- [17] Hyewon Suh et al. “No Significant Evolution of Relations between Black Hole Mass and Galaxy Total Stellar Mass Up to $z = 2.5$ ”. In: *The Astrophysical Journal* 889.1 (Jan. 20, 2020), p. 32. ISSN: 0004-637X, 1538-4357. DOI: [10.3847/1538-4357/ab5f5f](https://doi.org/10.3847/1538-4357/ab5f5f). URL: <https://iopscience.iop.org/article/10.3847/1538-4357/ab5f5f> (visited on 07/01/2025).
- [18] Mar Mezcua et al. “Overmassive Black Holes at Cosmic Noon: Linking the Local and the High-redshift Universe”. In: *The Astrophysical Journal Letters* 966.2 (May 1, 2024), p. L30. ISSN: 2041-8205, 2041-8213. DOI: [10.3847/2041-8213/ad3c2a](https://doi.org/10.3847/2041-8213/ad3c2a). URL: <https://iopscience.iop.org/article/10.3847/2041-8213/ad3c2a> (visited on 07/01/2025).
- [19] Ignas Juodžbalis et al. *JADES: comprehensive census of broad-line AGN from Reionization to Cosmic Noon revealed by JWST*. ADS Bibcode: 2025arXiv250403551J. Apr. 1, 2025. DOI: [10.48550/arXiv.2504.03551](https://doi.org/10.48550/arXiv.2504.03551). URL: <https://ui.adsabs.harvard.edu/abs/2025arXiv250403551J> (visited on 07/01/2025).
- [20] C. Giménez-Arteaga et al. “Outshining in the spatially resolved analysis of a strongly lensed galaxy at $z = 6.072$ with JWST NIRCam”. In: *Astronomy & Astrophysics* 686 (June 2024), A63. ISSN: 0004-6361, 1432-0746. DOI: [10.1051/0004-6361/202349135](https://doi.org/10.1051/0004-6361/202349135). URL: <https://www.aanda.org/10.1051/0004-6361/202349135> (visited on 07/01/2025).
- [21] Anna Ferré-Mateu et al. “On the formation mechanisms of compact elliptical galaxies”. In: *Monthly Notices of the Royal Astronomical Society* 473.2 (Jan. 11, 2018), pp. 1819–1840. ISSN: 0035-8711. DOI: [10.1093/mnras/stx2442](https://doi.org/10.1093/mnras/stx2442). URL: <https://doi.org/10.1093/mnras/stx2442> (visited on 07/01/2025).
- [22] Mar Mezcua et al. “Overmassive Black Holes in Dwarf Galaxies Out to $z = 0.9$ in the VIPERS Survey”. In: *The Astrophysical Journal Letters* 943.1 (Jan. 1, 2023), p. L5. ISSN: 2041-8205, 2041-8213. DOI: [10.3847/2041-8213/acae25](https://doi.org/10.3847/2041-8213/acae25). URL: <https://iopscience.iop.org/article/10.3847/2041-8213/acae25> (visited on 07/01/2025).